

To assess the mechanical properties, the complete elastic constant tensor (C_{ij}) was calculated for TiFeTe and its Se-alloyed systems. From these data, the bulk modulus (B), shear modulus (G), Young's modulus (Y), Pugh's ratio (B/G), Poisson's ratio (ν), and acoustic velocities were derived to evaluate the mechanical stability and stiffness of the crystals¹⁻⁵. The calculated parameters are summarized in Table 1.

Table 1. Mechanical Parameters of TiFeTe and Its Alloying

parameter	TiFeTe	TiFeTe _{0.75} Se _{0.25}	TiFeTe _{0.5} Se _{0.5}	TiFeTe _{0.25} Se _{0.75}
C11(Gpa)	293.298	293.945	293.575	292.169
C12(Gpa)	89.467	93.834	98.433	105.070
C44(Gpa)	66.659	68.855	70.789	75.278
B(Gpa)	157.411	160.538	163.480	167.436
G(Gpa)	75.724	76.959	77.929	79.721
Y(Gpa)	195.778	199.068	201.731	206.405
B/G	2.079	2.086	2.098	2.100
ν	0.2927	0.2933	0.2943	0.2945
v_l (m/s)	5834.91	5966.12	6080.08	6207.85
v_t	3158.82	3226.42	3282.38	3350.16
v	3525.09	3600.81	3663.73	3739.48
Θ_D (K)	319.82	321.96	339.40	345.65
(γ)	1.728	1.732	1.738	1.739
Kl(slack)	24.775	19.509	21.164	20.755

Furthermore, the lattice thermal conductivity (κ_l) was preliminarily estimated using the Slack model⁶, which, despite its approximate nature, effectively captures the influence of alloying on phonon transport within limited computational resources. Subsequently, more accurate calculations of κ_l were conducted using VASP, thirddorder.py, and ShengBTE, allowing for detailed analysis of phonon scattering and heat transport mechanisms.

table 2. Relaxation Time Data of TiFeTe and Its Alloying System

Compound	Carrier type	E_β (eV)	C (eV/Å ³)	$m^*(m_e)$	τ (fs)
TiFeTe	Electron	12.47	1.798	0.609	135.35
	Hole	12.23	1.798	1.429	39.14
TiFeTe _{0.75} Se _{0.25}	Electron	12.39	1.773	0.635	127.34
	Hole	11.78	1.773	1.337	47.53
TiFeTe _{0.5} Se _{0.5}	Electron	12.48	1.826	0.632	130.39
	Hole	12.44	1.826	1.331	42.94
TiFeTe _{0.25} Se _{0.75}	Electron	-12.32	1.711	0.747	97.57
	Hole	-11.39	1.711	1.423	43.42

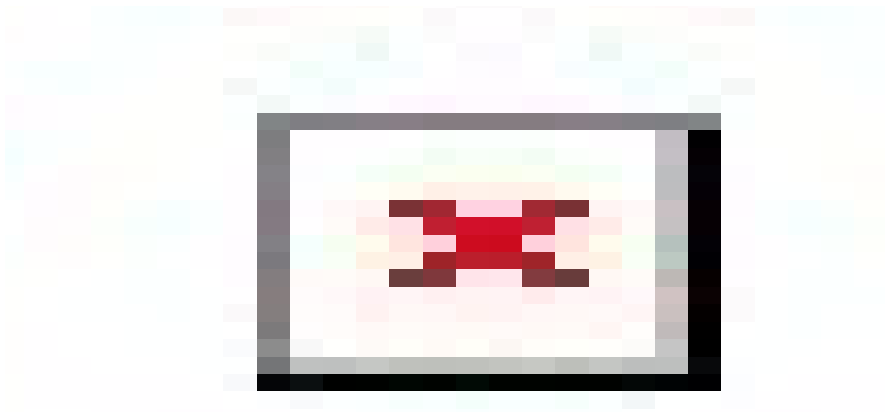


Figure 1. Comparison of the changes in the energy band by the DFT+U correction .

We performed a comparative assessment of the PBE–GGA results and those obtained with the DFT+U correction. Upon introducing +U, the band gap increases, while the overall band dispersions and their temperature-relevant features remain essentially unchanged (Fig. 1). Consistently, the calculated electronic transport quantities, including the Seebeck coefficient and the electrical conductivity(Fig. 2), show only minor variations between PBE and PBE+U. Importantly, these small changes in the electronic structure and electronic transport do not affect the lattice thermal conductivity, and therefore do not alter our main conclusion that Se alloying effectively suppresses κ_1 via enhanced phonon scattering.

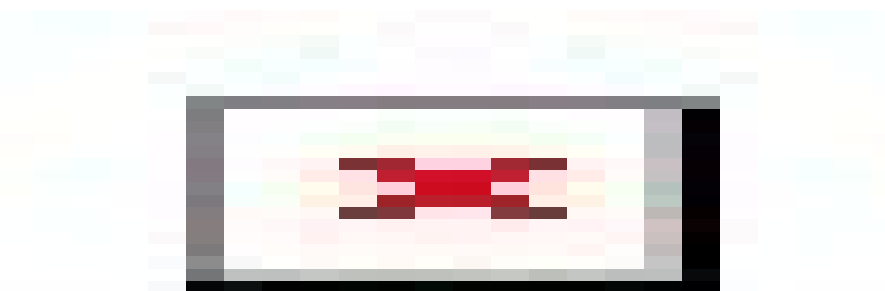


Figure 2. Comparison of the changes in electrical transport properties by the DFT+U correction

We assessed thermodynamic stability using Materials Project data for the end members. TiFeTe is predicted to be stable on the convex hull with $E_{\text{above hull}}=0.000$ eV/atom, whereas TiFeSe lies 0.195 eV/atom above the hull and is predicted to decompose into $\text{Ti}_3\text{Se}_4+\text{TiFe}+\text{Fe}$, indicating a significant driving force for decomposition toward the Se-rich end member at 0 K.^{10.1063/1.4812323} Since Materials Project does not provide entries for intermediate alloy compositions $\text{TiFeTe}_{1-x}\text{Se}_x$, we further evaluated alloying thermodynamics via ordered supercell calculations and

computed the mixing energy $\Delta E_{\text{mix}}(x)$ referenced to the linear interpolation between TiFeTe and TiFeSe end members (Fig. 3). The composition-dependent ΔE_{mix} suggests a tendency toward phase separation (or metastability) in parts of the composition range; nevertheless, there are no imaginary frequencies in the phonon spectrum calculations of these two systems. configurational entropy at finite temperature may stabilize solid solutions, making experimental realization plausible.

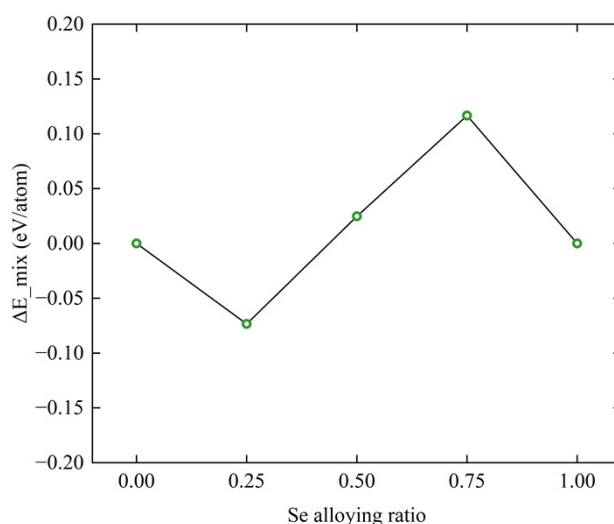


Figure 3. Mixing energy ΔE_{mix} of ordered $\text{Ti}_4\text{Fe}_4\text{Te}_{4-n}\text{Se}_n$ supercells as a function of Se fraction x , referenced to the linear interpolation between $\text{Ti}_4\text{Fe}_4\text{Te}_4$ and $\text{Ti}_4\text{Fe}_4\text{Se}_4$ (PBE). Positive ΔE_{mix} indicates a 0 K driving force toward phase separation relative to the end members, whereas negative values suggest energetically favorable mixing for the chosen ordered configuration.

Notes and references

- (1) Chen, X.-Q.; Niu, H.; Li, D.; Li, Y. Modeling Hardness of Polycrystalline Materials and Bulk Metallic Glasses. *Intermetallics* **2011**, *19* (9), 1275–1281. <https://doi.org/10.1016/j.intermet.2011.03.026>.
- (2) Fine, M. E.; Brown, L. D.; Marcus, H. L. Elastic Constants versus Melting Temperature in Metals. *Scr. Metall.* **1984**, *18* (9), 951–956. [https://doi.org/10.1016/0036-9748\(84\)90267-9](https://doi.org/10.1016/0036-9748(84)90267-9).
- (3) Nazarenko, L. V. Elastic Properties of Materials with Ellipsoidal Pores. *Int. Appl. Mech.* **1996**, *32* (1), 46–52. <https://doi.org/10.1007/BF02084847>.
- (4) Pugh, S. F. XCII. Relations between the Elastic Moduli and the Plastic Properties of Polycrystalline Pure Metals. *Lond. Edinb. Dublin Philos. Mag. J. Sci.* **1954**, *45* (367), 823–843. <https://doi.org/10.1080/14786440808520496>.
- (5) Soga, N.; Anderson, O. L. Simplified Method for Calculating Elastic Moduli of Ceramic Powder from Compressibility and Debye Temperature Data. *J. Am. Ceram. Soc.* **1966**, *49* (6), 318–322. <https://doi.org/10.1111/j.1151-2916.1966.tb13272.x>.
- (6) Morelli, D. T.; Slack, G. A. High Lattice Thermal Conductivity Solids. In *High Thermal Conductivity Materials*; Shindé, S. L., Goela, J. S., Eds.; Springer-Verlag: New York, 2006; pp 37–68. https://doi.org/10.1007/0-387-25100-6_2.